Energy 299 (2024) 131197

Contents lists available at ScienceDirect

Energy

journal homepage: www.elsevier.com/locate/energy

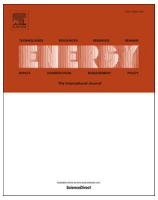

Experimental investigation of the CO_2+$SiCl_4$ mixture as innovative working fluid for power cycles: Bubble points and liquid density measurements

M. Doninelli [a,*], E. Morosini [b], G. Di Marcoberardino [a], C.M. Invernizzi [a], P. Iora [a], M. Riva [c], P. Stringari [c], G. Manzolini [b]

[a] Università degli Studi di Brescia, Dipartimento di Ingegneria Meccanica ed Industriale, via Branze, 38, 25123, Brescia, Italy
[b] Politecnico di Milano, Dipartimento di Energia, Via Lambruschini 4A, 20156, Milano, Italy
[c] Mines Paris, PSL University, Centre of Thermodynamics of Processes (CTP), 77300, Fontainebleau, France

ARTICLE INFO

Keywords:
CO_2 mixtures
sCO_2
CSP
Vapour-liquid equilibrium
Liquid density
Working fluids

ABSTRACT

Supercritical CO_2 is recognized as a promising working fluid for next-generation of high temperature power cycles. Nevertheless, the use of CO_2 mixtures with heavier dopants is emerging as a promising alternative to supercritical CO_2 cycles in the recent years for air-cooled systems in hot environments. Accordingly, this work presents an experimental campaign to assess the thermodynamic behaviour of the CO_2+$SiCl_4$ mixture to be used as working fluid for high-temperature applications, conducted in the laboratories of CTP Mines Paris PSL. At first, bubble conditions of the mixture are measured in a variable volume cell (PVT technique), then liquid densities are measured with a vibrating tube densimeter, for molar composition in the range between 70 % and 90 % of CO_2. The Peng Robinson EoS was fine-tuned on the bubble points obtained, resulting in a satisfactory accuracy level. Finally, a non-conventional methodology has been developed to measure bubble points with the vibrating tube densimeter, whose results are consistent with the VLE data obtained with the standard PVT technique. Thermodynamic analysis in next-generation concentrated solar power plant, at 700 °C turbine inlet, confirms the mixture overcomes 50 % thermal efficiency, providing +4.2 % net electrical output over pure supercritical CO_2 at equal thermal power from the solar field.

1. Introduction

Starting from the theoretical conceptualization of supercritical CO_2 (sCO_2) power cycles attributed to Angelino [1] and Feher [2], a renewed and growing interest in this technology has been experienced in the last decade, especially to replace the state-of-the-art steam Rankine cycle in innovative categories of power generation systems. In particular, sCO_2 as working fluid is considered attractive in high-temperature applications such as nuclear [3], concentrated solar power (CSP) [4,5], hybrid plants [6], and high-temperature waste heat and heat recovery [7–9], mainly due to high thermodynamic efficiencies, also at part load conditions [10].

However, when considering applications with air-cooled heat rejection units (HRU) in environments with high average ambient temperatures, such as CSP locations, the effectiveness of sCO_2 cycles is negatively influenced by the higher compressibility factor of the CO_2 across the compression step, caused by the high compression inlet temperature (up to 50 °C). High values of cycle minimum temperature can also be adopted for cogeneration purposes, in order to deliver heat to a thermal user such as for district heating networks [11] or thermal desalination plants [12].

For this reason, H2020 European-funded projects such as the SCARABEUS project [13] and the DESOLINATION project [14] identified a possible solution to increase the cycle efficiency by varying the working fluid itself: in this circumstance the working fluid remains liquid across the whole compression step, entailing a low mechanical power consumption at any cycle minimum temperatures. To do so, CO_2-based mixtures are adopted in power cycles as working fluids: by mixing CO_2 with a dopant characterized by a high critical temperature it is possible to turn the supercritical cycle into a transcritical one. This solution can allow an increment of cycle efficiency with respect to sCO_2 cycles, especially when the cycle minimum temperature is as high as 50 °C (with ambient temperatures around 35 °C) [15]. The dopant molar fraction represents an additional degree of freedom of the power block which allows for the maximization of the electrical efficiency: depending on the specific dopant and power block layout the optimal mixture

* Corresponding author.
E-mail address: m.doninelli002@unibs.it (M. Doninelli).

https://doi.org/10.1016/j.energy.2024.131197
Received 21 December 2023; Received in revised form 28 March 2024; Accepted 2 April 2024
Available online 12 April 2024

compositions can be found in the 70–90 % range of CO_2 molar content [16]. For this reason, in this work, the CO_2 mixture is experimentally investigated in the above-mentioned composition range.

One of the most challenging factor that limits the widespread of the sCO_2 cycle technology is the design, manufacturing and operation of the main compressor: it must be designed to specifically work with CO_2 in near-critical conditions at its intake, where small temperature fluctuations can lead to non-negligible density variations and to the risk of the onset of liquid droplets as a consequence of the local acceleration near the blades leading edge [17].

On the other hand, the technological development of pumps operating with CO_2-based mixtures in liquid conditions theoretically appears as a minor technological challenge as attested by the pump manufactures involved in the H2020 DESOLINATION project [18]. Nevertheless, even if the compression of a liquid can be easier than a near-critical point compression of a supercritical fluid, a solid knowledge of the thermodynamic properties of the compressed flow is still necessary when innovative working fluids are considered (as binary mixtures with CO_2).

While selecting a CO_2-based mixture to be used as working fluid, a fundamental aspect in the dopant selection is its thermal stability, important to avoid decomposition products across the cycle that can lead to component malfunctions, accumulation of non-condensable products as well as engine blockage. The identification of fluids whose chemical bonds are not subjected to dissociation or isomerization reactions above 550 °C (i.e. the state-of-the-art maximum temperature for CSP plants with solar salts) is a challenging task. In fact, is it well-known that the maximum operating temperatures of the fluids commercially employed in Organic Rankine Cycles (ORC) is below 300–350 °C due to thermal stability issues [19]. For example, Siloxanes can be safely adopted in ORCs up to 260 °C [20], with acceptable decomposition rates, while hydrocarbons can operate near 300 °C [19] as maximum temperature. CO_2 binary mixtures with refrigerants have been studied by Sánchez and da Silva [21] for geothermal application, by Dai et al. [22] for low-grade heat conversion, as well as by Yao et al. [23] in medium-temperature waste heat recovery considering a maximum turbine inlet temperature of 360 °C. However, most of refrigerants cannot be considered as CO_2 dopant in state-of-the art CSP tower plants since refrigerants chemically decompose at temperatures lower than 425 °C [24] due to C–H bond cleavage. A CO_2+propane binary mixture was investigated by Ma et al. [25] and Niu et al. [26] in CSP application at 550 °C turbine inlet temperature, presenting promising results at temperatures above the ones for conventional applications of propane.

Nevertheless, within the SCARABEUS and DESOLINATION frameworks, this ambitious target of 550 °C has been reached by a handful of mixtures: for example, the CO_2 mixture with hexafluorobenzene (C_6F_6) was demonstrated to be thermally stable below 600 °C [8] in an Inconel 625 alloy vessel for 100 h.

Focusing strictly on CSP, the target for next-generation solar tower plants is set at operating with cycle maximum temperatures up to 700 °C [27,28], posing further challenges on the identification of thermo-chemically stable dopants. In this direction, sulphur dioxide (SO_2) has been identified [29] within the SCARABEUS project as potential CO_2 dopant, and the associated efficiency gain compared to pure CO_2 is proved also by Tafur-Escanta et al. [30]. Also titanium tetrachloride ($TiCl_4$) has been considered in past years both as potential CO_2 dopant [31] in the SCARABEUS project, for the 700 °C level, and as a pure fluid for high-temperature Rankine cycles [32]: since it is industrially oxidized at very-high temperatures (1500–2000 K) to produce TiO_2 [33], its thermal stability has been preliminary taken for granted in applications with maximum temperatures levels of 700 °C.

Similarly to $TiCl_4$, Silicon Tetrachloride ($SiCl_4$) has the same tetrahedral structure and a remarkably high thermal stability, considering the various industrial processes where it is commonly adopted [34,35]. Both metal tetrachlorides are not flammable but they hydrolyse under exposure with humid air, decomposing in hydrochloric acid (HCl): nevertheless, the kinetic of the decomposition process is much slower in case of $SiCl_4$, as observed during the experimental tests presented in this work, justifying the interest in this fluid for industrial applications if compared to $TiCl_4$. Consequently, this work analyses the thermodynamic properties of the CO_2+$SiCl_4$ mixture, potentially to be adopted as working fluid for very-high temperature transcritical power cycles with high minimum temperature. Silicon Tetrachloride was produced in the past by reacting SiO_2 and chlorine at 1300 °C [36]. According to reports, the pure form remains thermally stable even at 1200 °C and it is much less reactive than $TiCl_4$ [37]. Approximatively 18–20 tons [38] of $SiCl_4$ are produced as by-product per ton of solar-grade silicon, reflecting the high market availability, the low cost, and the maturity of the industrial sector in handling this chemical component.

The objective of this research is to experimentally investigate the thermodynamic properties of the CO_2+$SiCl_4$ mixture as a novel working fluid for high-temperature power cycles. The primary aim is to assess the phase behaviour of the binary system, which is essential for determining thermodynamic conditions, designing components, and analysing off-design scenarios. Secondly, liquid density data of the mixture are necessary for future pump design and manufacturing.

The methodology involves conducting experimental studies to measure vapour-liquid equilibrium (VLE) data and liquid densities of the mixture. Two different apparatuses are employed: a Pressure-Volume-Temperature (PVT) apparatus for measuring bubble points and a vibrating tube densimeter (VTD) [39–41] for determining liquid densities across a wide pressure range.

Starting from the experimental data, an optimization procedure for a cubic Equation of State (EoS) is proposed. This involves fitting the binary interaction parameter (BIP) of the mixture using the Peng Robinson EoS [42], ensuring consistency across the different compositions measured.

Additionally, a non-conventional approach is developed to measure bubble points using vibrating tube densimeter. This approach provides data consistent with conventional method, validating the overall experimental methodology.

Finally, cycle calculations with fine-tuned EoS are performed to assess the performance of the CO_2+$SiCl_4$ mixture in next-generation CSP applications, at 700 °C maximum cycle temperature. These calculations are part of the H2020 DESOLINATION project, aiming to assess the potential advantages of the mixture over pure sCO_2 in terms of cycle thermal efficiency.

2. Experimental campaign for mixture characterisation: methodology and measurements

2.1. PVT apparatus: bubble points measurements

The bubble points reported in this work for the CO_2+$SiCl_4$ mixture have been measured at the Centre of Thermodynamics of Processes (CTP) of Mines Paris PSL in Fontainebleau, France, using the experimental apparatus previously presented by Neyrolles [43] and schematically reported in Fig. 1: it includes a variable volume cell (PVT), used to measure bubble points of pressurized mixtures as an alternative to a conventional and more complex VLE cell, equipped with a composition analysis system.

An accurate description of the PVT test rig adopted is proposed by Neyrolles [43] and it is summarized in this work. The core of the apparatus is a variable volume equilibrium cell consisting of a sapphire tube held between two titanium flanges with suitable O-rings. The volume of the cell can be varied by controlling the position of a piston in the upper part of the cell. The piston position is controlled by a motorized lead screw actuator from Thomson®. A Kollmorgen controller is used to precisely control the downward climb of the piston in the cell. The pressure and the temperature, as well as the piston position, are monitored in continuous. A 100 Ω platinum thermoresistance (PT-100) is adopted to measure the temperature in the lower part of the cell; the

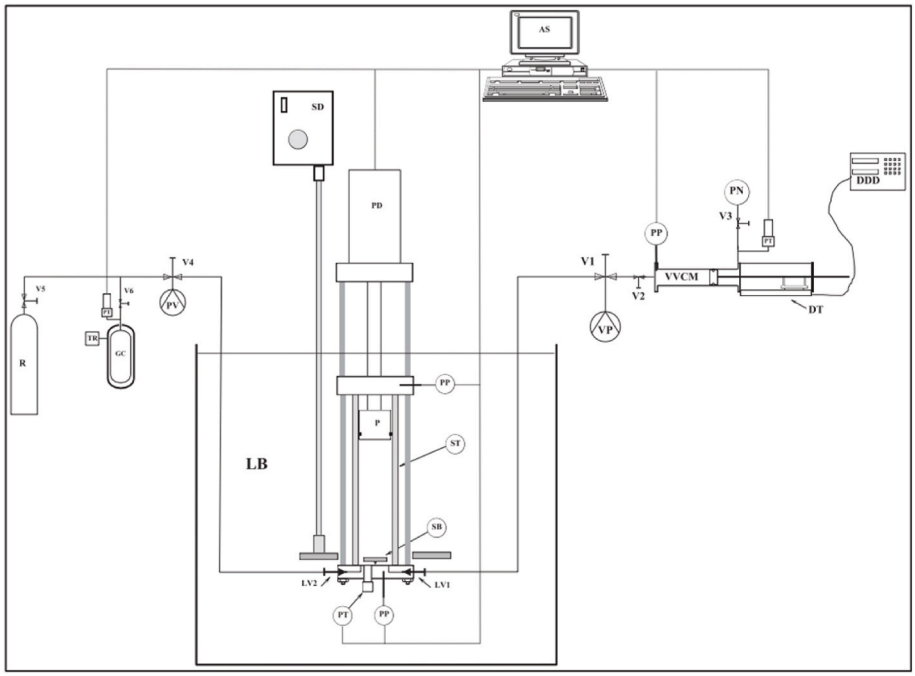

Fig. 1. Flow diagram of the apparatus. DDD: Digital Displacement Display; DT: Displacement Transducer; GC: Gas Cylinder; LB: Liquid Bath; LVi: Loading Valve; P: Piston; PD: Piston Monitoring; PN: Pressurized Nitrogen; PP: Platinum Probe; PT: Pressure Transducer; PV (VP): Vacuum Pump; R: Gas Reservoir; SD: Stirring Device; SB: Stirring Bar; ST: Sapphire Tube; TR: Thermal Regulator; Vi: Valve; VVCM: Variable Volume Cell with mechanical displacement of the piston. [43].

temperature sensor has been calibrated in comparison with a reference 25 Ω platinum probe (Tinsley, France), and the resulting accuracy is estimated to be ±0.03 K. The pressure is measured with a cryogenic miniature ruggedized Kulite pressure transducer placed at the bottom of the cell. The pressure transducer is calibrated with a precision pressure controller (Pace 5000 by Druck) in the range from 2 to 110 bar, and the resulting average accuracy was estimated to be ±26 mbar at the temperatures of interest. The measurements are carried out in isothermal conditions, since the cell is placed in a thermostatic water-based Tamson bath and the temperature set-point is guaranteed by a PID controller. The equilibrium conditions of the mixture in the cell are favoured by the presence of a corrosion-resistant magnetic stirrer placed at the cell bottom, which is controlled by an external agitator placed inside the bath. The mixture of CO_2 with $SiCl_4$ was vented under hood after neutralization into a water and Sodium Hydroxide (NaOH) solution to avoid the formation of HCl.

A detail of the variable volume cell can be visualized in Fig. 2: the piston and the sapphire cell are visible in the centre, the two agitators (one inside the cell and the second one, the actuator, out of the cell) in the bottom.

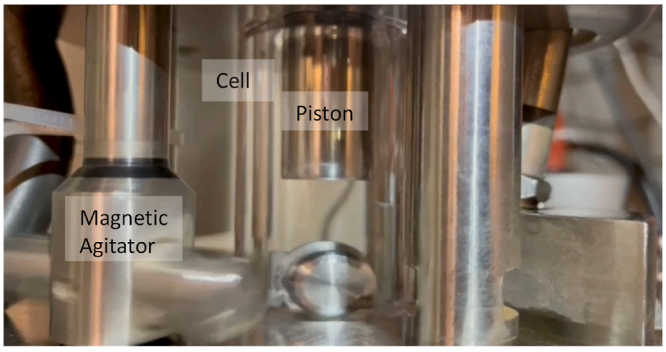

Fig. 2. High-pressure liquid mixture of CO_2+$SiCl_4$ after charging into the PVT cell, with agitation active.

Fig. 3 provides a better understading of the procedure adopted to identify each bubble point of the mixture with the PVT apparatus. At isothermal conditions, the position of the piston and the stabilized pressure inside the cell are recorded and plotted, as shown in Fig. 3, for a particular mixture composition and bath temperature.

The pressure variation measured in the cell is very significant if the mixture is at liquid conditions, where the mixture compressibility is very limited. On the other hand, in the VLE region, the pressure of the mixture is little sensitive to the volume variation because its effect on the pressure is compensated by the high compressibility of the gas phase. From the intersection of the two straight lines regressing the stabilized pressures as function of the piston displacement, detailing the pressure-volume behaviour of the mixture in both conditions (VLE and subcooled liquid), it is possible to determine the bubble pressure at the given fixed test temperature and mixture composition. Each bubble point (P,T,x) is experimentally evaluated at least three times in the PVT apparatus, both starting from the liquid and the VLE conditions: the different colours of

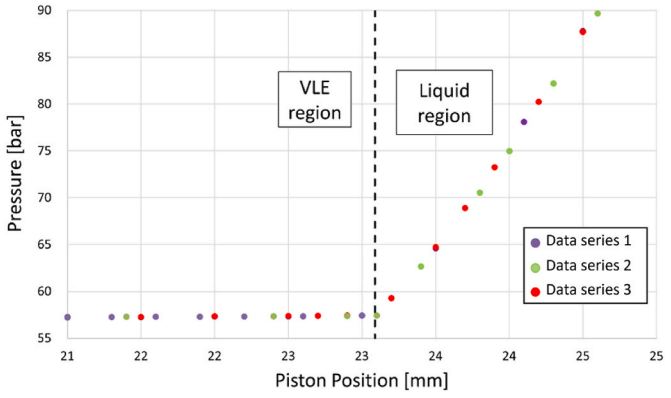

Fig. 3. PVT acquisitions for 80.2 % molar CO_2+$SiCl_4$ at 35 °C; different colours represent different series of measurements. (For interpretation of the references to colour in this figure legend, the reader is referred to the Web version of this article.)

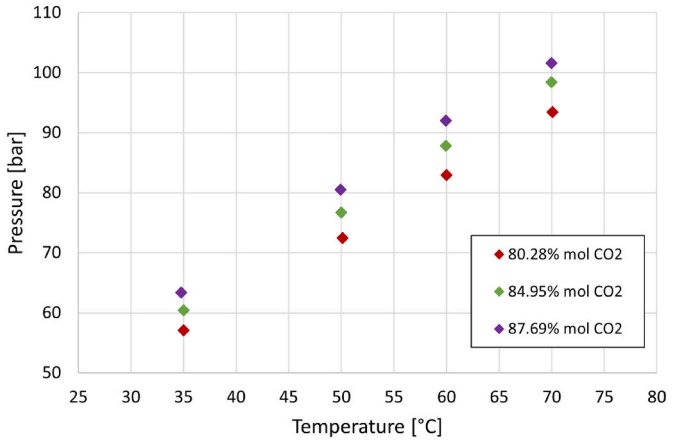

Fig. 4. Experimental bubble points for the mixture CO_2+$SiCl_4$.

the dots in Fig. 3 represent different measurement series. Each point in Fig. 3 represents a condition at which the piston position has been maintained fixed until the pressure is stabilized.

The experimental bubble points of the CO_2+$SiCl_4$ mixture are reported in Supplementary Data and represented in Fig. 4, taken in a composition range (80%–90 %) that are of interest for the application of the mixture as working fluid in a transcritical power cycle. For each composition, the bubble pressure has been measured at four temperatures (35 °C, 50 °C, 60 °C, 70 °C). In particular, bubble pressures at 50 °C and above are representative of bubble conditions at pump inlet of air-cooled power cycles in hot environments. The uncertainties on the temperature and the bubble pressure measured are reported together with the experimental values in Supplementary Data.

2.2. Vibrating tube densimeter

Liquid density measurements of the CO_2+$SiCl_4$ mixture have been obtained at the laboratory of the Center of Thermodynamics of Processes (CTP) of Mines Paris PSL by using a vibrating tube densimeter (VTD), which core is an Anton Paar DMA HPM, as described in literature [44]. The scheme of the apparatus is shown in Fig. 5.

The measurement procedure consists in determining the density of the liquid mixture from the variation of the vibration period of a U-shaped tube when it is filled with the fluid with respect to when it is at vacuum conditions. In order to convert the vibration period into density values, the vibration period of the tube filled with a fluid with a known density must be measured in the same experimental apparatus to define a correlation between the vibration period and the density. As this relation is temperature-dependent, this calibration must be carried out at each temperature of interest.

The VTD is immersed in a thermostatic liquid bath to maintain its temperature at a target value during the measurements. The operating range of the densimeter is from −10 °C to 200 °C in temperature, and over 1000 bar in pressure. The vibrating tube is made in Hastelloy, and its temperature is controlled by a heat transfer fluid flowing in a jacket with a temperature stability of 0.02 °C. Additional information about the VTD adopted can be found in a previous literature work [39]. During the operation and before arriving at the bubble point condition, reached by expanding the fluid from subcooled liquid conditions, the temperature of the thermostatic bath is kept around 0.2 °C lower than the heat transfer fluid flowing in the jacket of the densimeter, since the first bubble of CO_2-mixture must occur precisely into the vibrating tube.

A detail of the apparatus (the variable volume cylinder, the open thermostatic bath, and the pressure transducers of the VTD) is also proposed in Fig. 6.

The variable volume cell at the outlet of the VTD has been added to manually modify the density (and the pressure) of the measured fluid in the vibrating tube, without influencing the mixture in the variable volume cylinder: the modification has been proposed specifically for mixtures, since it is crucial to definitively fix the composition of the measured fluid, for various pressure levels. Accordingly, the position of the piston of the variable volume cell is manually modified (with valve V6 open) to match the pressure in the VTD to the desired value: once equilibrium is reached the valve V6 is closed and another acquisition can be carried out, at the same temperature but different pressure than the previous ones.

The described procedure is followed for each temperature at which measurements are carried out.

It is important to underline that the specific experimental set-up described in this work, with a variable volume cell before the venting of the mixture, is adopted to specifically measure the density of a binary mixture composed by two compounds with very different volatility. In this setup, the volume can be opportunely varied with a manual hip-pump. On the other hand, the most commonly adopted set-up to analyze the density of pure fluids or non-complex mixtures does not include the variable-volume cell at the VTD outlet (between V6 and the vent valve V7). With the conventional setup, after charging the mixture from high-pressure liquid conditions into the system, the vent valve (V7) is opened for a continuous evacuation (several seconds). This approach can be used because, when charging the pressurized mixture into the VTD at vacuum conditions, an initial flash is unavoidable: homogeneous mixture conditions are then reached by a continuous evacuation of the mixture through the vent valve. However, within this work it has been found out that subsequent sets of measurements of the same mixture (after venting it) were not repeatable due to a composition variation caused by the mixture flash after venting. For this reason, it was decided to collect the initial flash in the variable volume cell, instead of venting it out with the risk of compromising the mixture's composition inside the VTD.

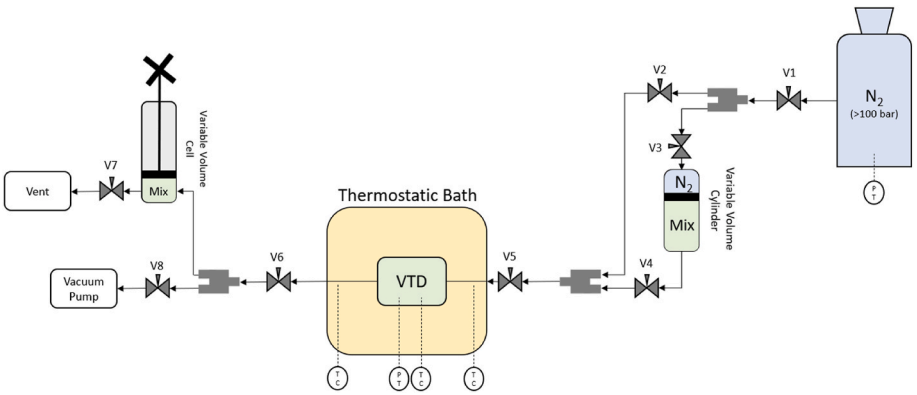

Fig. 5. Schematization of the test-rig adopted with the vibrating tube densimeter.

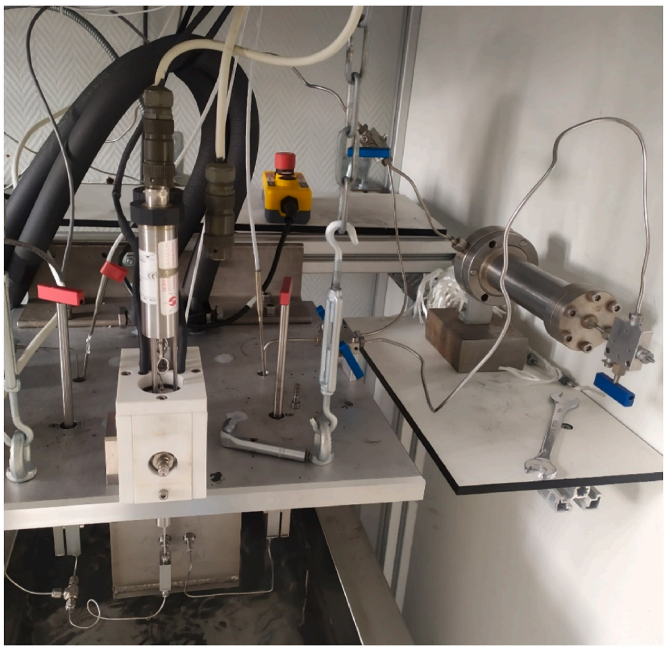

Fig. 6. Detail of the VTD apparatus, with the pressurized cylinder containing the mixture (on the right side), the red valves corresponding to the inlet/outlet valve of the VTD, the pressure transducers on the top, and the vibrating tube in its jacket above the free surface of the thermostatic bath. (For interpretation of the references to colour in this figure legend, the reader is referred to the Web version of this article.)

2.2.1. VTD: liquid density measurements

Densities are determined by calibrating the vibrating tube period (τ) with the known density of pure carbon dioxide (adopted as reference fluid) at 40 °C, 60 °C and 80 °C, with a linear correlation as reported in Equation (1):

$$\rho|_T = f(\tau)_T = A \cdot \tau + B \quad (1)$$

To build the correlation of Equation (1) for each temperature, the results of the equation of state by Span and Wagner [45] have been assumed as reference values to be associated with the measured vibrating periods, computing the numerical values of A and B for each temperature investigated with a linear interpolation. The uncertainty range of the Span and Wagner EoS with respect to CO_2 density ranges from 0.03 % to 0.05 % at pressures up to 30 MPa and temperature up to 523 K.

Three compositions of the CO_2+$SiCl_4$ mixture have been tested in the VTD: the results are reported in Supplementary Data and shown in Fig. 7.

For each series of measurements, at isothermal conditions, the minimum pressure investigated was chosen around 20 bar above the expected bubble or dew pressure at the tested temperature, in order to avoid the onset of vapour-liquid conditions. In addition, by varying the volume of the variable volume cylinder (in Fig. 5) with the hip-pump it was possible to investigate pressures above the one of the pressurized cylinder of the mixture.

2.2.2. VTD: bubble points measurements with innovative procedure

While analysing the CO_2+$SiCl_4$ mixture in the densimeter, a set of bubble points has been also determined with an innovative method. The operating principle that allows for the determination of the bubble condition using the VTD relies on the drastic variation of the oscillation period of the tube occurring while entering in the two-phase region starting from a condition of single-phase liquid at high pressure.

Two different procedures were adopted to reduce the pressure in the VTD and to approach the bubble pressure at isothermal conditions: both (i) by acting on the vent valve (V7 in Fig. 5), and alternatively (ii) by increasing the available volume of the mixture through the hip-pump variable-volume at the outlet of the system. The main difference between the two techniques is that in the first case there is a continuous mass flow in the system, while in the second option the mass flow is intermittent due to discontinuous volume variation.

An example of the bubble onset identification by acting on the vent valve V7 is represented in Fig. 8, monitoring the pressure and the vibrating tube oscillation period along the timespan considered. The pressure is reduced within the tube by around 0.05 bar per second, on average, controlling the needle valve at the vent. As the pressure reduces slowly down to the bubble condition at the set temperature, the oscillating period rapidly increases because of the formation of the vapour-phase that rapidly migrates towards the vent while the U-tube is enriched by the heavier liquid phase.

On the other hand, in Fig. 9 is proposed the determination of the bubble point of the mixture using the second procedure (manual hip-

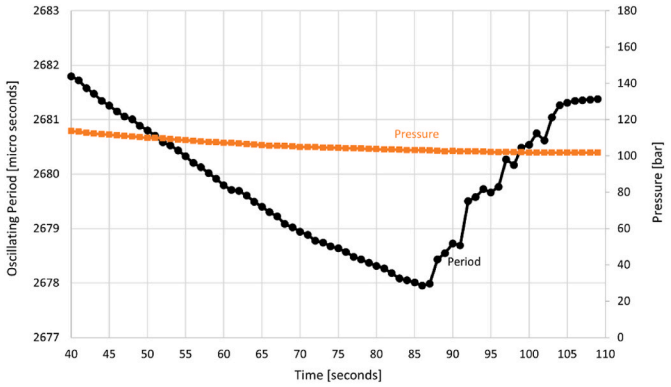

Fig. 8. Example of bubble point determination at the VTD acting on the vent valve.

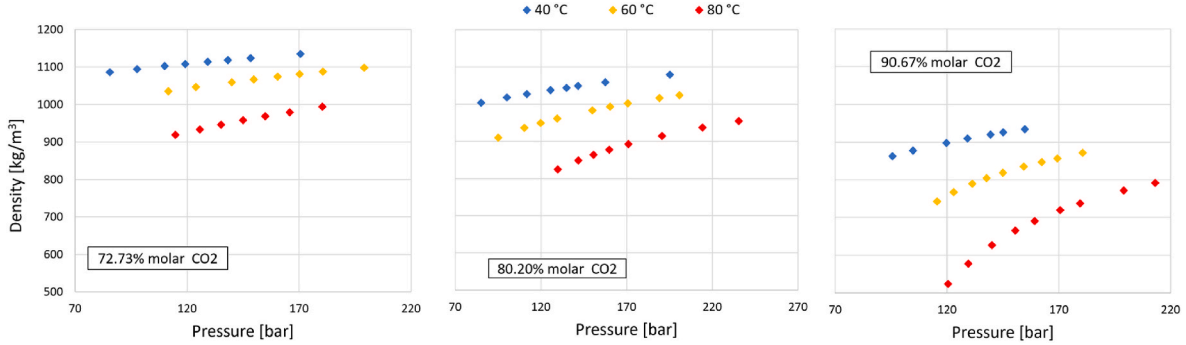

Fig. 7. Experimental liquid densities of CO_2+$SiCl_4$ mixture at different compositions at three different temperatures.

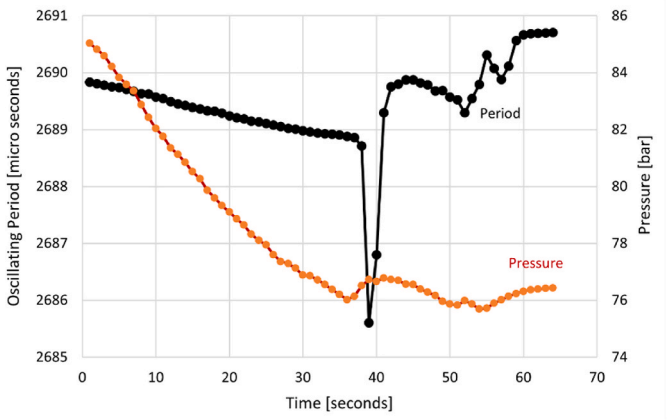

Fig. 9. Example of bubble point determination at the VTD acting on the manual hip-pump.

pump).

In this case, the bubble point can be more easily visualized due to a drastic drop in the oscillating period: the formation of a less-dense vapour phase rich in CO_2 accumulates into the tube and the period decreases consequently. At the same time, the local pressure increases since the volume occupied by the vapour phase increases. After a few seconds, acting on the hip-pump, the vapour phase tends to migrate from the tube to the variable-volume at the tube outlet, located at a higher geodetic level. Finally, due to the migration of the vapour-phase outside the tube, the fluid inside the tube remains the liquid phase that is rich in the dense dopant ($SiCl_4$) and the period starts increasing again.

The pressure reduction in the U-tube is less pronounced by using the vent valve than the hip-pump, resulting in a higher accuracy of the identified bubble pressure.

Even if the proposed approach strongly depends on the manual capacities of the operator dealing with the valve or the hip-pump, the collected data can also be treated in a semi-quantitative way by using the first or second derivative of the oscillating period against time. In particular, the bubble points at the VTD have been identified as stationary point or inflection point of the oscillating period, depending on the procedure used. An example of identification of the instant in which the first bubble forms within the U-tube can be found in Fig. 10, where the bubble onset is presented as a stationary point of the oscillating period with respect to the sampling time.

The bubble points obtained with the VTD apparatus are reported in Supplementary Data. The consistency of these additional points is validated in the following section.

3. Modelling and discussion

Reliable thermodynamic models are necessary to calculate the properties of binary mixtures along the thermodynamic regions of interest for the closed thermodynamic cycle. In the last decades, cubic EoS such as the Peng Robinson (PR) [42] and Soave-Redlich-Kwong (SRK) [46] have become consolidated choices, especially in the industry [47, 48]. Accordingly, in this work the original PR EoS [42] has been considered for a preliminary post-processing of the experimental data and thermodynamic analysis of the CO_2+$SiCl_4$ mixture. The PR EoS is expressed as in Eqs. (2)–(6):

$$P = \frac{RT}{v-b} - \frac{\alpha a}{v(v+b)+b(v-b)} \tag{2}$$

where the alpha function adopted is in its original form [42]:

$$\alpha = \left[1 + k\left(1 - \sqrt{T_r}\right)\right]^2 \tag{3}$$

$$k = 0.37464 + 1.54226\omega - 0.26992\omega^2 \tag{4}$$

$$a = 0.45724\frac{R^2 T_{cr}^2}{P_{cr}} \tag{5}$$

$$b = 0.0778\frac{RT_{cr}}{P_{cr}} \tag{6}$$

van der Waals mixing rules are then adopted to describe the binary mixture.

The EoS parameters of the chemical species studied in this work are reported in Table 1.

The binary interaction parameter (BIP) of the mixture has been regressed on the measured bubble points of the CO_2+$SiCl_4$ mixture. As a matter of fact, the accurate calibration of the EoS on VLE data is widely accepted in scientific literature as the best way to approach, at least at the first stage, the optimization of the EoS. The BIP regression is performed within the software ASPEN Properties v12 [49], using the maximum likelihood method as numerical optimization method. Even if bubble points have been obtained also with the VTD, the regression is

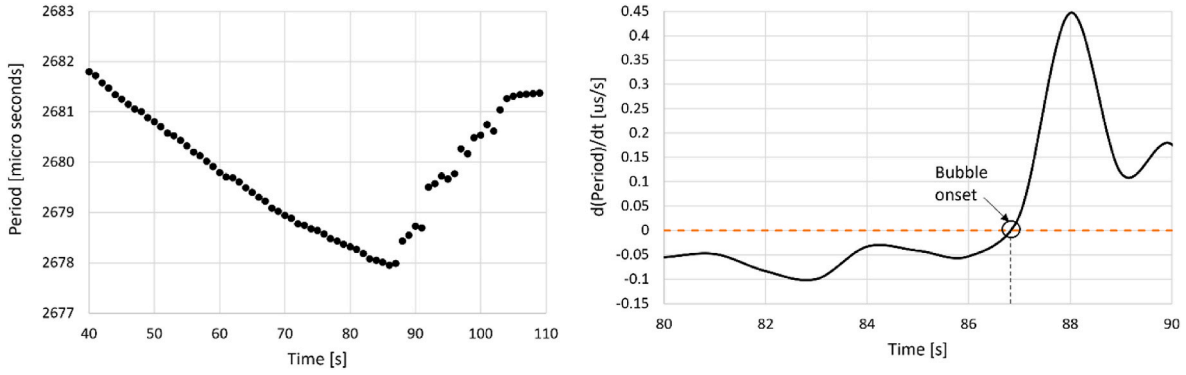

Fig. 10. Example of identification of the bubble point onset from the first derivative of the oscillating period against time.

Table 1
Parameters used in the EoS (default values in ASPEN [49] Properties).

Fluid	Critical temperature [°C]	Critical pressure [bar]	Pitzer's acentric factor ω [−]
CO_2	31.06	73.83	0.2236
$SiCl_4$	233.85	35.9	0.2318

Table 2
Binary interaction parameter regressed and AAD% of the PR EoS for CO_2+$SiCl_4$ mixture.

EoS	k_{ij}	*AAD: bubble pressure*				
		35 °C	50 °C	60 °C	70 °C	Global
PR	*0.06098 ± 0.00338*	*0.57 %*	*0.56 %*	*0.56 %*	*1.00 %*	*0.68 %*

carried out only considering the data measured with the PVT apparatus. In order to assess the accuracy in fitting the VLE properties, the average absolute deviation percentage (AAD%) was chosen as an index to quantify the accuracy of the EoS in representing the experimental data. The AAD is computed in this work as shown in Equation (7), where P_{exp} is the measured pressure, P_{calc} is the pressure calculated by using the EoS, and N is the number of experimental data considered:

$$AAD_{Pbubble}[\%] = \frac{100}{N} \cdot \sum_{i=1}^{n} \left| \frac{P_{exp} - P_{calc}}{P_{exp}} \right| \quad (7)$$

Table 2 reports the binary interaction parameter (k_{ij}) obtained by the data regression in ASPEN Plus v12 and the AAD% computed on the bubble pressure for each temperature, along with an overall average AAD% on all conditions. The Britt–Luecke algorithm [50] with Deming [51] initialization method was applied to regress the parameter.

The PR EoS with optimized binary interaction parameter can represent the VLE data of this mixture, obtained with PVT apparatus, with good precision, as indicated by the AAD%. In Fig. 11, the experimental bubble data from this work are shown as diamonds, while the resulting VLE curves obtained by the PR EoS with the regressed BIP are shown as solid lines.

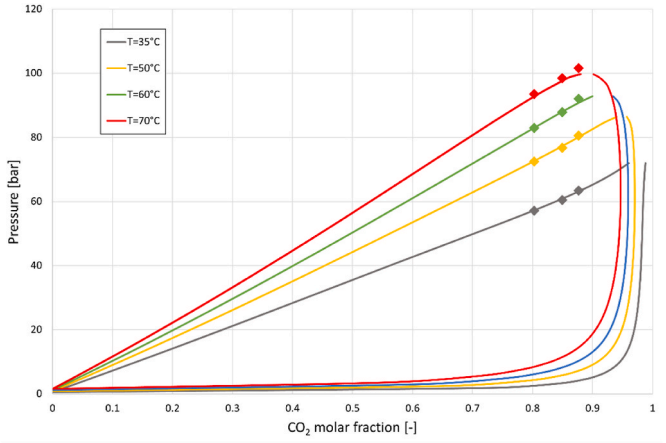

Fig. 11. Pressure-composition diagram of CO_2+$SiCl_4$ mixture with the optimized PR EoS (solid lines) at the four isothermal test conditions, dots represent the experimental data obtained in this work with the PVT apparatus.

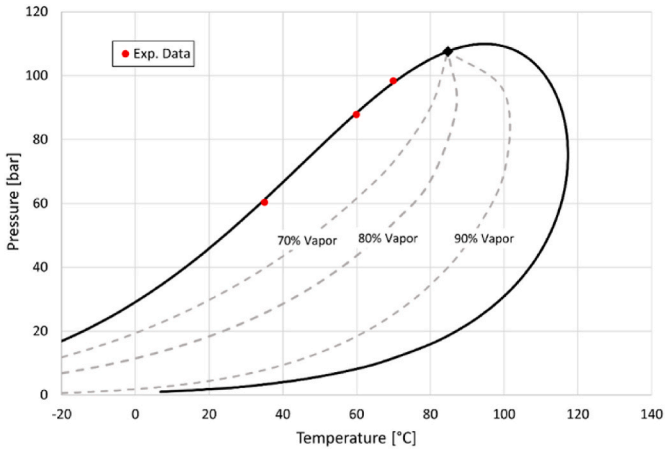

Fig. 12. Phase envelope of a 85 % molar CO_2 mixture with $SiCl_4$; PR EoS calculations (solid line), calculated critical point (black dot), calculated vapour quality curves (dashed lines), and experimental bubble points (red dots). (For interpretation of the references to colour in this figure legend, the reader is referred to the Web version of this article.)

Another representation of the mixture two-phase behaviour is also possible in a pressure-temperature chart, as the one in Fig. 12 for a CO_2 molar composition of 85 %. A temperature glide of about 65 °C can be seen at 80 bars, while the critical point is far enough from the pump inlet operating conditions (slightly subcooled liquid at around 50–60 °C).

In Fig. 13, the bubble points obtained using the densimeter (with the methodology shown in section 2.3.2) are reported as red dots on the phase envelopes corresponding to the experimental compositions (solid lines) calculated with the PR EoS optimized only on the bubble point data obtained using the PVT apparatus. On the left part of Fig. 13, it is possible to visualize the consistency between the bubble points obtained with two different charges at almost the same composition (80.28 % molar for the mixture tested at the PVT, 80.2 % molar for the mixture tested at the VTD) with the two methodologies.

As evident from Fig. 13, the additional bubble points obtained using the VTD are consistent with those obtained with the rigorous PVT method and with the bubble lines computed using the PR EoS optimized only on the PVT data. The method proposed can be useful to have a preliminary knowledge of vapour-liquid phase boundaries of multicomponent systems without the requirement of expensive VLE dedicated apparatus, at least as a preliminary step.

The capability of the PR EoS with the regressed value of the BIP to predict the liquid densities of the mixture was tested, resulting in an AAD of 2.22 %, considering all the data collected. The comparison between the optimized PR EoS and the experimental liquid densities of the mixture (Supplementary Data and Fig. 7) is presented in Table 3.

The PR EoS shows good agreement at higher $SiCl_4$ content (AAD =

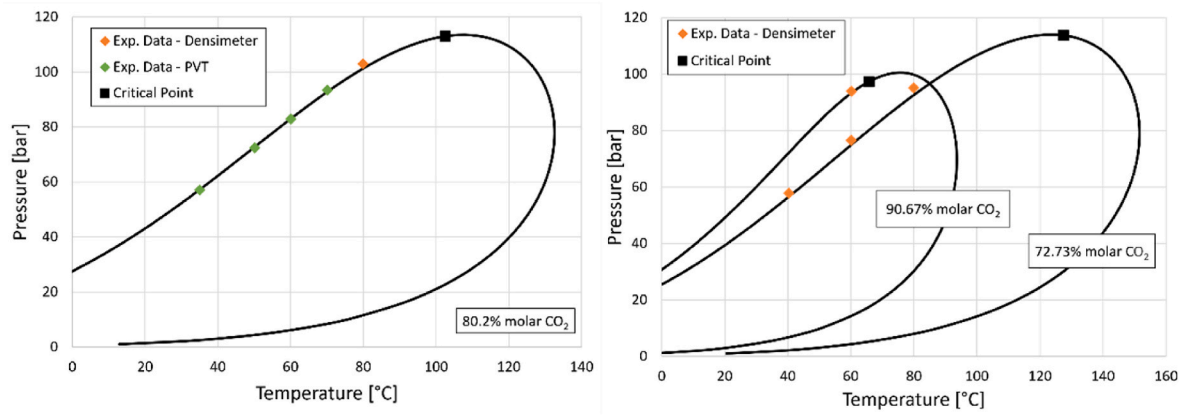

Fig. 13. P-T envelope curves of CO_2+$SiCl_4$ mixtures (solid lines) and critical points (black points) calculated with the optimized PR EoS, and experimental bubble points measured using the densimeter (red points) and the PVT (green points). (For interpretation of the references to colour in this figure legend, the reader is referred to the Web version of this article.)

Table 3
Average absolute deviation percent of the PR EoS with K_{ij} against liquid densities of CO_2+$SiCl_4$ mixture.

	AAD [%]			
CO_2 molar fraction %	40 °C	60 °C	80 °C	Average
72.7 %	2.16	0.74	0.84	1.26
80.2 %	1.19	1.90	1.34	1.49
90.7 %	2.16	5.47	3.67	3.89

1.26 % for 72.73 % CO_2 molar content) while it underestimates the liquid densities at higher CO_2 molar content (AAD = 3.89 % for 90.67 % CO_2 molar fraction). It must be noted that at 90.67 % CO_2 molar fraction the calculated critical point is 64.4 °C, and the higher deviations encountered at 60 °C are probably attributed to near critical point conditions.

3.1. Comparison with previous literature works

In literature, other studies on this binary system are found and a comparison is proposed here, but a wider examination can be found in Supplementary Data. In Fig. 14, large deviations are present between the measured bubble points with the PVT apparatus and the data reported only in graphical form in Suleimenov [52].

The results from the Peng Robinson EoS with the binary interaction parameter regressed in this work have been compared with a second set

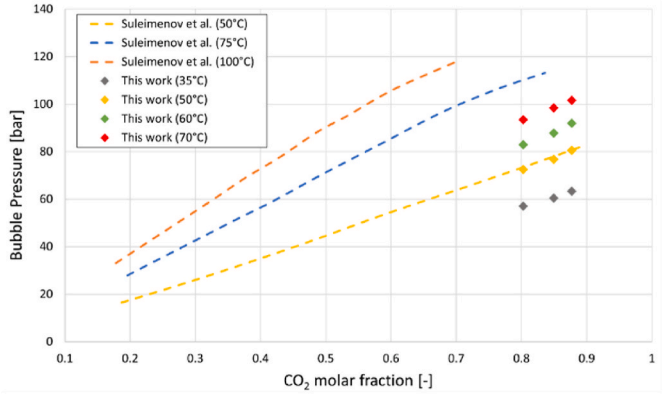

Fig. 14. Comparison between the bubble points measured in this work (dots) and the smoothed bubble line as reported by Suleimenov et al. [52] for the mixture CO_2 + $SiCl_4$.

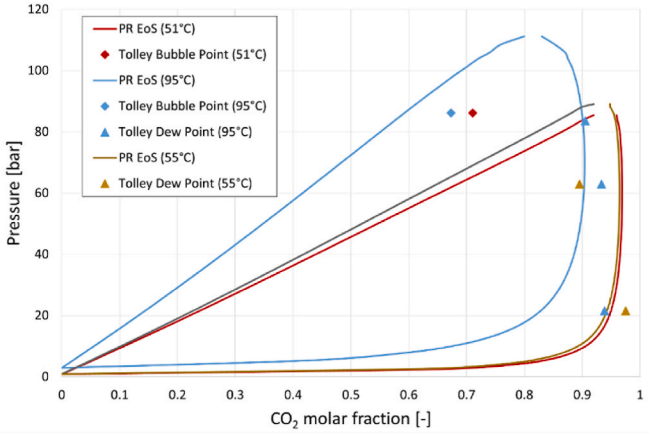

Fig. 15. Comparison between the PR EoS (solid lines) fitted with data obtained in this work and the experimental data reported in Tolley et al. [53].

of experimental data available in literature from Tolley's master thesis [53]. The graphical comparison between the EoS and Tolley data is reported in Fig. 15, evidencing lack of agreement.

The comparison between the results of this work and those previously presented in literature evidenced large discrepancy, stressing the specific experimental investigation carried out for the CO_2+$SiCl_4$ mixture.

4. Preliminary analysis of CO_2+$SiCl_4$ power cycle in CSP context

This last section is dedicated to preliminary estimate the performance of the innovative CO_2+$SiCl_4$ mixture as working fluid for transcritical cycles for very high temperature CSP plants, justifying the interest in the experimental investigation proposed in this work. The EoS adopted to model the mixture and its BIP is the one proposed in this work in Table 2.

The cycle calculations consider a maximum temperature of 700 °C, compatible with the expected thermal stability of the working fluid mixture and coherent with next-generation of central tower CSP plants. Such thermal level is also compatible with liquid HTFs to be adopted in high temperature external tubular receivers above 700 °C, with sodium [54] or innovative mixtures [55] as HTF and innovative molten salts as storage fluids.

The thermodynamic cycle is simulated in Aspen Plus, considering the adoption of the CO_2+$SiCl_4$ mixture and sCO_2 in a recompression layout, which is the most effective layout for sCO_2 [56] due to balanced heat

Table 4
Power cycles assumptions and non-idealities for sCO_2 and CO_2 mixture cycles.

Power Cycle Parameter	Value
Turbine Inlet Temperature [°C]	700
Maximum Cycle Pressure [bar]	250
Cycle Minimum Temperature [°C]	50
Turbine/Compression Isentropic Efficiency [%]	92/88
PCHE Minimum Internal Temperature Difference [°C]	5
Condenser/HRU Pressure loss [%]	2
PHE Pressure loss [%]	2
PCHE Pressure loss HP/LP [%]	0.3/1.5
Expander electro-mechanical efficiency [%]	98
Pump/Compressor electro-mechanical efficiency [%]	98
Fans (HRU) Electrical Consumption [MW_{el}]	1 % Q_{HRU}

capacities in the recuperators. To evaluate the pure sCO_2 cycle, both the PR EoS and the Span-Wagner EoS [45] as implemented in REFPROP v10 [57] are used. The use of the PR EoS for both mixture and pure sCO_2 is necessary to fairly compare the two working fluids under the same thermodynamic model. The Span-Wagner EoS is also considered for the sCO_2 case as it is recognized to be the ad advanced and effective model to calculate the thermodynamic properties of CO_2. Compared to pure sCO_2, the CO_2+$SiCl_4$ mixture can benefit from liquid phase pumping instead of using the primary compressor, due to transcritical conditions. To solve the thermodynamic cycles some assumptions on the non-idealities of the components are used and reported in Table 4, according with previous literature work [29], and considered valid both for the sCO_2 cycle and the transcritical CO_2+$SiCl_4$ cycle. The cycle minimum temperature is assumed to be 50 °C, representing an air-cooled design condition in hot-environments, typical of CSP plants.

The layout adopted for the mixture is reported in Fig. 16, with the associated temperature-entropy (T-s) diagram of the CO_2+$SiCl_4$ mixture cycle considering a 92 % CO_2 molar content. Referring to the recompression layout in Fig. 16, the pre-heating section is divided into two recuperators, operating at different temperatures, i.e. low-temperature (LT) and high-temperature (HT) printed circuit heat exchangers (PCHEs), managing distinct mass flow rates to counterbalance the varying heat capacities of the CO_2-based fluid within the heat recovery process.

The adoption of a transcritical power cycle in recompressed layout require the mixture to work in single-phase conditions at the exit of the low-temperature printed circuit heat exchanger recuperator (PCHE LT), points 9-10-11 in Fig. 16, to provide dry conditions at the (secondary) compressor inlet. For this mixture and the conditions considered at the compression inlet, this is verified only for CO_2 molar content above 90 % due to a reduction in the temperature glide occurring during the nearly isobaric condensation. A sensitivity test on the CO_2 molar fraction has been carried out from 90 % to 100 % CO_2, providing an overview of the effects of the mixture composition on the thermodynamic cycle efficiency, defined as in Equation (8).

$$\eta_{Cycle} = \frac{W_{Turbine} - W_{Main\ Pump/Compressor} - W_{Re-Compressor}}{Q_{PHE}} \tag{8}$$

As evident from Fig. 17, the CO_2+$SiCl_4$ mixture outperforms pure CO_2 in thermodynamic efficiency: at around 92 % CO_2 molar fraction, the 50 % efficiency target is reached with the mixture in transcritical conditions, enabling around +1.3 % efficiency point compared to pure sCO_2 (a relative deviation of around 2 % in mechanical power at constant thermal input). The mixture does not only demonstrate an enhanced cycle efficiency with respect to the sCO_2 cycle, but it also allows a reduction of approximately 25 °C of the temperature at the

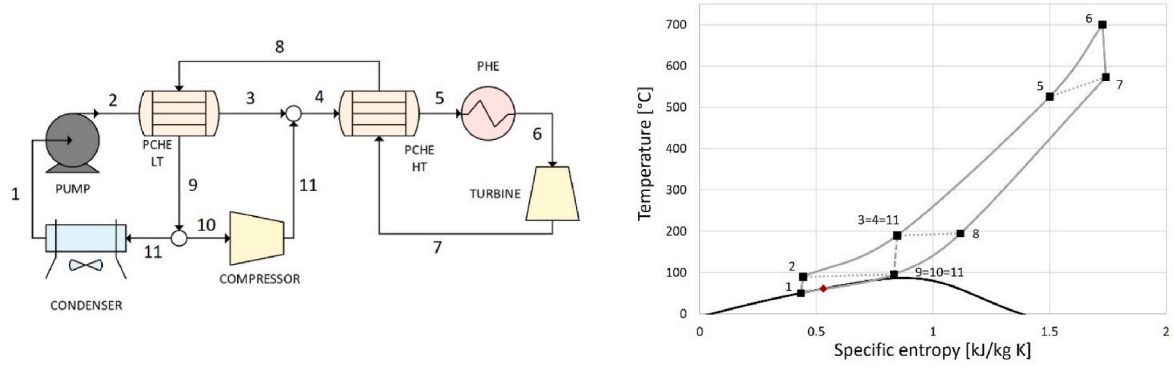

Fig. 16. Recompression power block layout (left side) for the transcritical CO_2+$SiCl_4$ mixture and associated T-s diagram (right side). The critical point of the mixture is represented as a red diamond in the T-s diagram. The internal heat recovery processes (LT and HT PCHE) is represented through dotted lines, while the recompressor as dashed line. (For interpretation of the references to colour in this figure legend, the reader is referred to the Web version of this article.)

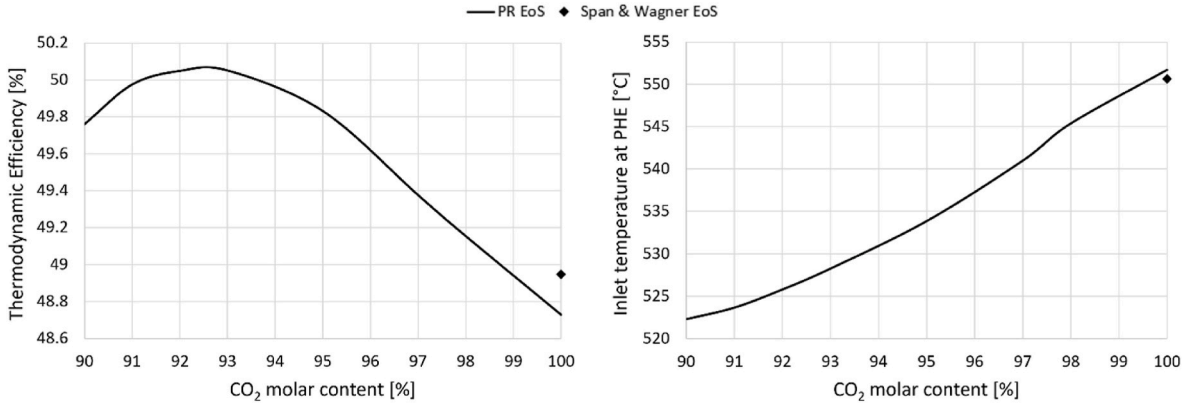

Fig. 17. Thermodynamic cycle efficiency of CO_2+$SiCl_4$ and sCO_2 in recompressed layout (left), and temperature of the working fluid at the inlet of the PHE (right).

Table 5
Performance of CO_2+$SiCl_4$ and sCO_2 power cycles at design conditions, for 100 MW gross mechanical output.

Variable	sCO_2 Cycle	CO_2+$SiCl_4$ Cycle
Plant layout	Recompressed	Recompressed
CO_2 molar fraction [−]	1	0.92
Mass Flow Rate [kg/s]	1086.3	1016
Pump/Main Compressor Power [MW]	28.6	19.7
Recompressor Power [MW]	18.2	15.6
Turbine Power [MW]	146.8	135.3
Recuperator Thermal Power [MW]	128.5 (LT) - 498 (HT)	121.2 (LT) – 405.3 (HT)
PHE Thermal Power [MW]	205.2	199.8
HRU Thermal Power [MW]	105.2	99.8
UA LT PCHE Recuperator [MW/K]	22.3	22.6
UA HT PCHE Recuperator [MW/K]	18.5	17
Working fluid inlet PHE Temperature [°C]	551.7	525.7
Thermodynamic Cycle Efficiency [%]	**48.73**	**50.05**
Electromechanical losses [MW_{el}]	3.3	3
HRU Fan Consumption [MW_{el}]	1.1	1
HTF Pump Consumption [MW_{el}]	1	0.8
Cycle Electric Efficiency [%]	**46.1**	**48.1**

primary heat exchanger's inlet (PHE). As a result, it becomes possible to decrease the return temperature of the heat transfer fluid (HTF), subsequently reducing the parasitic electrical consumption of the HTF pump (having a lower mass flow rate at fixed thermal power).

Above 95 % CO_2 molar fraction, the mixture works in supercritical conditions, as pure sCO_2, but the benefits of increasing the critical temperature are still present. In fact, even if the highest efficiency is identified at transcritical conditions (due to the low compression work at liquid conditions), the supercritical compression of the mixture at nearer critical conditions provides for better efficiency than pure sCO_2 (critical temperature 31 °C). This is a consequence of the real gas effects, which are less pronounced in the case of sCO_2 due to the higher temperature difference between the compression inlet and the fluid critical point. The minimum pressure of the transcritical cycles working with the CO_2 mixture is the bubble pressure at pump inlet (50 °C), while it is an optimized parameter in case of sCO_2 and for the mixture above 95 % CO_2 molar content.

Considering the results of the innovative cycle at the optimized composition of 92 % CO_2 molar, a comparison with the pure sCO_2 cycle is presented in Table 5, for a gross mechanical power of 100 MW. The comparison is presented in terms of both thermodynamic and electrical efficiency, considering the parasitic consumptions of the HTF pump, the auxiliary fans of an air-cooler at the heat rejection unit (HRU), and the electro-mechanical losses (see Table 4).

In Table 5, the evaluation of the electrical consumption of the HTF pump as function of the temperature at the inlet of the PHE follows the methodology presented in a previous literature work [58], considering sodium as HTF and considering a solar multiple of the CSP plant from the literature of around 2.7, if adopting the thermodynamic cycles of this work in Table 4.

It can be noted that the net electrical efficiency of the mixture cycle results to be +2 % efficiency points higher than pure CO_2, which is significant for the revenues and the economic performance of a CSP plant, and it represents an increment of around 4.2 % in electric power at constant thermal input (considering the same solar plant).

5. Conclusions

In this work, experimental bubble points and liquid densities of a CO_2-rich mixture (more than 70 % molar content) with $SiCl_4$ as dopant have been measured to assess the phase behaviour and volumetric behaviour of the mixture as potential working fluid in transcritical power cycles. The bubble point data obtained with a variable-volume PVT apparatus can be used in future works for calibrating proper equations of state and evaluating the cycle conditions, optimizing the performance. From a preliminary analysis, the Peng Robinson EoS with regressed BIP showed a good accuracy in representing the experimental bubble points (AAD of 0.68 %), while acceptable deviations (AAD of 2.22 %) are found with respect to the measured high-pressure liquid densities.

The particular set-up adopted for the vibrating tube densimeter resulted to be determinant for the measurement of the density of the CO_2+$SiCl_4$ mixture, characterized by large differences in volatility between the two components. As an innovative outcome of this work, the VTD was used not only to measure liquid densities of the mixture, but also to obtain additional bubble points. The bubble points acquired at VTD resulted to be consistent with those from the PVT test rig, as well as with the thermodynamic model optimized only on the data from the PVT. This procedure can be adopted in the future to have preliminary information about the VLE conditions of a mixture.

The comparison with previous literature works highlighted the discrepancies of the data available in the literature, justifying even more the experimental campaign carried out here.

A preliminary thermodynamic analysis carried out with the optimized EoS demonstrates the potentiality of this mixture in comparison to pure sCO_2 in power cycles under the same assumptions and power block configuration (recompression layout), enabling a net electrical efficiency gain of around +2 % points in a next-generation CSP tower plant with 700 °C turbine inlet temperature. The mixture also allows for a reduction of approximately 25 °C in the temperature at the primary heat exchanger's inlet, also decreasing the return temperature of the HTF, thereby mitigating the parasitic electrical losses resulting from HTF pump operations. Notably, the net electrical output of the CO_2+$SiCl_4$ mixture cycle in a CSP plant presents a +4.2 % point increment over pure CO_2, under the same thermal power from the solar field, making a significant impact on the revenues and overall economic performance of a concentrated solar power plant.

CRediT authorship contribution statement

M. Doninelli: Writing – original draft, Visualization, Validation, Software, Methodology, Investigation, Formal analysis, Data curation, Conceptualization. **E. Morosini:** Writing – original draft, Visualization, Validation, Software, Methodology, Investigation, Formal analysis. **G. Di Marcoberardino:** Validation, Supervision, Investigation, Writing – review & editing. **C.M. Invernizzi:** Supervision, Visualization, Writing – review & editing. **P. Iora:** Visualization, Supervision, Project administration, Resources. **M. Riva:** Writing – original draft, Validation, Supervision, Resources, Methodology, Investigation, Formal analysis. **P. Stringari:** Writing – original draft, Supervision, Resources, Methodology, Investigation, Formal analysis. **G. Manzolini:** Supervision, Resources, Project administration, Investigation, Funding acquisition.

Declaration of competing interest

The authors declare that they have no known competing financial interests or personal relationships that could have appeared to influence the work reported in this paper.

Data availability

Data will be made available on request.

Acknowledgements

This paper is part of the DESOLINATION project that has received funding from the European Union's Horizon 2020 research and innovation programme under grant agreement No 101022686.

Appendix A. Supplementary data

Supplementary data to this article can be found online at https://doi.org/10.1016/j.energy.2024.131197.

Nomenclature

Acronyms

AAD	Average Absolute Deviation
CSP	Concentrated solar power
EoS	Equation of state
HT	High Temperature
HTF	Heat Transfer Fluid
HRU	Heat Rejection Unit
LT	Low Temperature
ORC	Organic Rankine Cycle
PCHE	Printed Circuit Heat Exchanger
PHE	Primary Heat Exchanger
PR	Peng Robinson EoS
PVT	Pressure-Volume-Temperature
VLE	Vapour-Liquid Equilibrium
VTD	Vibrating Tubr Densimeter

Symbols

b	Covolume
P	Pressure, bar
ρ	Density, kg m^{-3}
Q	Thermal Power, MW
T	Temperature, °C
v	Specific Volume
W	Mechanical Power, MW

Greek symbols

α	Alpha Function of the EoS
τ	Period, s
ω	Pitzer acentric factor

Subscripts

cr	Critical
el	Electrical

References

[1] Angelino G. Carbon dioxide condensation cycles for power production. J. Eng. Power. 1968;90:287–95. https://doi.org/10.1115/1.3609190.

[2] Feher EG. The supercritical thermodynamic power cycle. Energy Convers 1968;8 (2):85–90.

[3] Dostal V, Hejzlar P, Driscoll MJ. High-performance supercritical carbon dioxide cycle for next-generation nuclear reactors. Nucl Technol 2006;154:265–82. https://doi.org/10.13182/NT154-265.

[4] Crespi F, Sánchez D, Rodríguez JM, Gavagnin G. A thermo-economic methodology to select sCO2 power cycles for CSP applications. Renew Energy 2020;147: 2905–12. https://doi.org/10.1016/j.renene.2018.08.023.

[5] Binotti M, Astolfi M, Campanari S, Manzolini G, Silva P. Preliminary assessment of sCO2 cycles for power generation in CSP solar tower plants. Appl Energy 2017;204: 1007–17. https://doi.org/10.1016/j.apenergy.2017.05.121.

[6] Alenezi A, Vesely L, Kapat J. Exergoeconomic analysis of hybrid sCO2 Brayton power cycle. Energy 2022;247:123436. https://doi.org/10.1016/j.energy.2022.123436.

[7] Manente G, Fortuna FM. Supercritical CO2 power cycles for waste heat recovery: a systematic comparison between traditional and novel layouts with dual expansion. Energy Convers Manag 2019;197:111777. https://doi.org/10.1016/j.enconman.2019.111777.

[8] Wright SA, Davidson CS, Scammell WO. Thermo-economic analysis of four sCO2 waste heat recovery power systems. 5th Int. Symp. - Supercrit. CO2 Power Cycles 2016:1–16.

[9] Gotelip T, Gampe U, Glos S. Optimization strategies of different SCO2 architectures for gas turbine bottoming cycle applications. Energy 2022;250:123734. https://doi.org/10.1016/j.energy.2022.123734.

[10] Alfani D, Binotti M, Macchi E, Silva P, Astolfi M. sCO2 power plants for waste heat recovery: design optimization and part-load operation strategies. Appl Therm Eng 2021;195:117013. https://doi.org/10.1016/j.applthermaleng.2021.117013.

[11] Morosini E, Doninelli M, Alfani D, Astolfi M, Di Marcoberardino G, Manzolini G. Analysis of the potential of Co2 based mixtures to improve the efficiency of cogenerative waste heat recovery power plants. Conf. Proc. Eur. SCO2 Conf. 2023: 169–78. https://doi.org/10.17185/duepublico/77287.

[12] Doninelli M, Morosini E, Gentile G, Putelli L, Di Marcoberardino G, Binotti M, Manzolini G. Thermal desalination from rejected heat of power cycles working with CO2-based working fluids in CSP application: a focus on the MED technology. Sustain Energy Technol Assessments 2023;60:103481. https://doi.org/10.1016/j.seta.2023.103481.

[13] Binotti M, Di Marcoberardino G, Iora P, Invernizzi C, Manzolini G. Scarabeus: supercritical carbon dioxide/alternative fluid blends for efficiency upgrade of solar power plants. AIP Conf Proc 2020;2303. https://doi.org/10.1063/5.0028799.

[14] DESOLINATION – Sustainable desalination from Concentrated Solar Power., (n.d.). https://desolination.eu/.

[15] Di Marcoberardino G, Morosini E, Manzolini G. Preliminary investigation of the influence of equations of state on the performance of CO2 + C6F6 as innovative working fluid in transcritical cycles. Energy 2022;238:121815. https://doi.org/10.1016/j.energy.2021.121815.

[16] Crespi F, de Arriba P, Sánchez D, Ayub A, Di Marcoberardino G, Invernizzi C, Martínez GS, Iora P, Di Bona D, Binotti M, Manzolini G. Thermal efficiency gains enabled by using CO2 mixtures in supercritical power cycles. Energy 2021;238: 121899. https://doi.org/10.1016/j.energy.2021.121899.

[17] Romei A, Gaetani P, Persico G. Computational fluid-dynamic investigation of a centrifugal compressor with inlet guide vanes for supercritical carbon dioxide power systems. Energy 2022;255:124469. https://doi.org/10.1016/j.energy.2022.124469.

[18] Terracciano OA, De Francesco F, Brizzi R, Annese F, Doninelli M, Putelli L, Gelfi M. An advanced desalination system with an innovative CO2 power cycle integrated with renewable energy sources. D011S017R002 2023. https://doi.org/10.2118/215993-MS.
[19] Invernizzi CM, Iora P, Manzolini G, Lasala S. Thermal stability of n-pentane, cyclopentane and toluene as working fluids in organic Rankine engines. Appl Therm Eng 2017;121:172–9. https://doi.org/10.1016/j.applthermaleng.2017.04.038.
[20] Keulen L, Gallarini S, Landolina C, Spinelli A, Iora P, Invernizzi C, Lietti L, Guardone A. Thermal stability of hexamethyldisiloxane and octamethyltrisiloxane. Energy 2018;165:868–76. https://doi.org/10.1016/j.energy.2018.08.057.
[21] Sánchez CJN, da Silva AK. Technical and environmental analysis of transcritical Rankine cycles operating with numerous CO2 mixtures. Energy 2018;142:180–90. https://doi.org/10.1016/j.energy.2017.09.120.
[22] Dai B, Dang C, Li M, Tian H, Ma Y. Thermodynamic performance assessment of carbon dioxide blends with low-global warming potential (GWP) working fluids for a heat pump water heater. Int J Refrig 2015;56:1–14. https://doi.org/10.1016/j.ijrefrig.2014.11.009.
[23] Yao Y, Shi L, Tian H, Wang X, Sun X, Zhang Y, Wu Z, Sun R, Shu G. Combined cooling and power cycle for engine waste heat recovery using CO2-based mixtures. Energy 2022;240:122471. https://doi.org/10.1016/j.energy.2021.122471.
[24] Angelino G, Invernizzi C. Experimental investigation on the thermal stability of some new zero ODP refrigerants. Int J Refrig 2003;26:51–8. https://doi.org/10.1016/S0140-7007(02)00023-3.
[25] Ma N, Bu Z, Fu Y, Hong W, Li H, Niu X. An operation strategy and off-design performance for supercritical brayton cycle using CO2-propane mixture in a direct-heated solar power tower plant. Energy 2023;278:127882. https://doi.org/10.1016/j.energy.2023.127882.
[26] Niu X, Ma N, Bu Z, Hong W, Li H. Thermodynamic analysis of supercritical Brayton cycles using CO2-based binary mixtures for solar power tower system application. Energy 2022;254:124286. https://doi.org/10.1016/j.energy.2022.124286.
[27] Mehos M, Turchi C, Vidal J, Wagner M, Ma Z, Ho C, Kolb W, Andraka C, Kruizenga A. Concentrating solar power Gen3 demonstration roadmap. Nrel/Tp-5500-67464 2017:1–140. https://doi.org/10.2172/1338899.
[28] He YL, Qiu Y, Wang K, Yuan F, Wang WQ, Li MJ, Guo JQ. Perspective of concentrating solar power. Energy 2020;198:117373. https://doi.org/10.1016/j.energy.2020.117373.
[29] Morosini E, Ayub A, di Marcoberardino G, Invernizzi CM, Iora P, Manzolini G. Adoption of the CO2 + SO2 mixture as working fluid for transcritical cycles: a thermodynamic assessment with optimized equation of state. Energy Convers Manag 2022;255. https://doi.org/10.1016/j.enconman.2022.115263.
[30] Tafur-Escanta P, López-Paniagua I, Muñoz-Antón J. Thermodynamics analysis of the supercritical CO2 binary mixtures for Brayton power cycles. Energy 2023;270. https://doi.org/10.1016/j.energy.2023.126838.
[31] Manzolini G, Binotti M, Bonalumi D, Invernizzi C, Iora P. CO2 mixtures as innovative working fluid in power cycles applied to solar plants. Techno-economic assessment. Sol Energy 2019;181:530–44. https://doi.org/10.1016/J.SOLENER.2019.01.015.
[32] Invernizzi CM, Iora P, Bonalumi D, Macchi E, Roberto R, Caldera M. Titanium tetrachloride as novel working fluid for high temperature Rankine Cycles: thermodynamic analysis and experimental assessment of the thermal stability. Appl Therm Eng 2016;107:21–7. https://doi.org/10.1016/j.applthermaleng.2016.06.136.
[33] West RH, Shirley RA, Kraft M, Goldsmith CF, Green WH. A detailed kinetic model for combustion synthesis of titania from TiCl4. Combust Flame 2009;156:1764–70. https://doi.org/10.1016/j.combustflame.2009.04.011.
[34] Okamoto Y, Sumiya M, Nakamura Y, Suzuki Y. Effective silicon production from SiCl4 source using hydrogen radicals generated and transported at atmospheric pressure. Sci Technol Adv Mater 2020;21:482–91. https://doi.org/10.1080/14686996.2020.1789438.
[35] Wan Y, Zhao X, Yan D, Yang D, Li Y, Guo S. Research and preparation of ultra purity silicon tetrachloride. AIP Conf Proc 2017;1890. https://doi.org/10.1063/1.5005228.
[36] Mochizuki Y, Bud J, Liu J, Tsubouchi N. Production of silicone tetrachloride from rice husk by chlorination and performance of mercury adsorption from aqueous solution of the chlorinated residue. ACS Omega 2020;5:29110–20. https://doi.org/10.1021/acsomega.0c03789.
[37] United States. Bureau of Mines. Mineral facts and problems. 1985 Edition. Washington D.C; 1985.
[38] Cheng C, Zhang C, Jiang J, Ma E, Bai J, Wang J. Raman spectroscopy characterization of dissolved polysilicon byproduct $SiCl_4$ in ionic liquids. J. Spectrosc. 2018;2018:2329189. https://doi.org/10.1155/2018/2329189.
[39] Thermodynamics JC, Stringari P, Scalabrin G, Valtz A, Richon D. Density measurements of liquid 2-propanol at temperatures between (280 and 393) K and at pressures up to 10 MPa. J Chem Thermodyn 2009;41:683–8. https://doi.org/10.1016/j.jct.2008.12.014.
[40] Stringari P, Scalabrin G, Richon D, Tecnica F, Tep CEP, Fre C, Saint Honore R. Compressed and saturated liquid densities for the 2-propanol + water system. 2008. p. 1789–95.
[41] Stringari P, Scalabrin G, Richon D, Coquelet C. Liquid density and bubble pressure measurements for the propylene + 2-propanol system. 2008. p. 1167–74.
[42] Peng DY, Robinson DB. A new two-constant equation of state. Ind Eng Chem Fundam 1976;15:59–64. https://doi.org/10.1021/i160057a011.
[43] Neyrolles E, Valtz A, Coquelet C, Chapoy A. On the phase behaviour of the CO2 + N2O4 system at low temperatures. Chem Eng Sci 2022;258:117726. https://doi.org/10.1016/j.ces.2022.117726.
[44] Nazeri M, Chapoy A, Valtz A, Coquelet C. Fluid Phase Equilibria New experimental density data and derived thermophysical properties of carbon dioxide e Sulphur dioxide binary mixture (CO 2 - SO 2) in gas , liquid and supercritical phases from 273 K to 353 K and at pressures up to 42 MPa. Fluid Phase Equil 2017;454:64–77. https://doi.org/10.1016/j.fluid.2017.09.014.
[45] Span R, Wagner W. A new equation of state for carbon dioxide covering the fluid region from the triple-point temperature to 1100 K at pressures up to 800 MPa. J Phys Chem Ref Data 1996;25:1509–96. https://doi.org/10.1063/1.555991.
[46] Soave G. Equilibrium constants from a modified Redlich-Kwong equation of state. Chem Eng Sci 1972;27:1197–203. https://doi.org/10.1016/0009-2509(72)80096-4.
[47] Lopez-Echeverry JS, Reif-Acherman S, Araujo-Lopez E. Peng-Robinson equation of state: 40 years through cubics. Fluid Phase Equil 2017;447:39–71. https://doi.org/10.1016/j.fluid.2017.05.007.
[48] Bertucco A, Fermeglia M. 50 years of Soave Equation of State (SRK): a source of inspiration for chemical engineers. Fluid Phase Equil 2023;566:113678. https://doi.org/10.1016/j.fluid.2022.113678.
[49] Aspen Technology Inc.. Aspen Plus®. 2022., Version V12.1.
[50] Britt HI, Luecke RH. The estimation of parameters in nonlinear, implicit models. Technometrics 1973;15:233–47. https://doi.org/10.1080/00401706.1973.10489037.
[51] Deming WE. Statistical adjustment of data. New York: Dover Publication Inc.; 1943.
[52] Suleimenov OM, Panagiotopoulos AZ, Seward TM. Grand canonical Monte Carlo simulations of phase equilibria of pure silicon tetrachloride and its binary mixture with carbon dioxide. Mol Phys 2003;101:3213–21. https://doi.org/10.1080/00268970310M.
[53] Tolley WK. Supercritical behavior of selected metal chlorides with carbon dioxide: a study of solubilities, solution densities, and excess enthalpies of mixing. 1990.
[54] Conroy T, Collins MN, Grimes R. Sodium receiver designs for integration with high temperature power cycles. Energy 2019;187:115994. https://doi.org/10.1016/j.energy.2019.115994.
[55] Manzolini G, Lucca G, Binotti M, Lozza G. A two-step procedure for the selection of innovative high temperature heat transfer fluids in solar tower power plants. Renew Energy 2021;177:807–22. https://doi.org/10.1016/j.renene.2021.05.153.
[56] Alfani D, Astolfi M, Binotti M, Silva P, Macchi E. Off-design performance of CSP plant based on supercritical CO2 cycles. AIP Conf Proc 2020;2303:130001. https://doi.org/10.1063/5.0029801.
[57] Lemmon EW, Bell Ian H, Huber ML, McLinden MO. NIST standard reference database 23: reference fluid thermodynamic and transport properties-REFPROP. National Institute of Standards and Technology; 2018. https://doi.org/10.18434/T4/1502528., Version 10.0.
[58] Morosini E, Villa E, Quadrio G, Binotti M, Manzolini G. Solar tower CSP plants with transcritical cycles based on CO2 mixtures: a sensitivity on storage and power block layouts. Sol Energy 2023;262:111777. https://doi.org/10.1016/j.solener.2023.05.054.